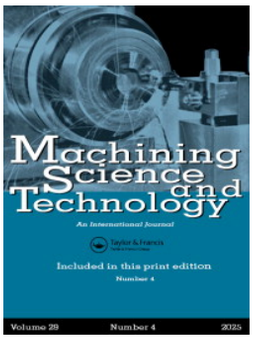

Taylor & Francis
Taylor & Francis Group

Machining Science and Technology
An International Journal

ISSN: 1091-0344 (Print) 1532-2483 (Online) Journal homepage: www.tandfonline.com/journals/lmst20

Optimization of numerical parameters in machining of Ti alloy

X. Soldani & Héctor López-Galvez

To cite this article: X. Soldani & Héctor López-Galvez (22 Aug 2025): Optimization of numerical parameters in machining of Ti alloy, Machining Science and Technology, DOI: 10.1080/10910344.2025.2541824

To link to this article: https://doi.org/10.1080/10910344.2025.2541824

MACHINING SCIENCE AND TECHNOLOGY
https://doi.org/10.1080/10910344.2025.2541824

Taylor & Francis
Taylor & Francis Group

Optimization of numerical parameters in machining of Ti alloy

X. Soldani[a] and Héctor López-Galvez[b]

[a]Department of Mechanical Engineering - ICAI, Universidad Pontificia Comillas, Madrid, Spain; [b]Grupo JPG, Madrid, Spain

ABSTRACT

Numerical models applied to the machining of titanium alloys are essential tools in the aerospace industry, as they help reduce the need for extensive and costly experimental trials while enabling precise analysis of complex machining phenomena. This work focuses on the optimization of numerical parameters in a finite element model of high-speed orthogonal cutting applied to Ti6Al4V, using the Abaqus software. Particular attention is given to the influence and calibration of numerical parameters (such as mesh size and mass scaling factor), along with tribological (friction at the tool/chip interface) and material-related parameters (fracture energy of the workpiece material), over a wide range of cutting speeds. The objective is to enhance the reliability and accuracy of the model in predicting key machining outputs such as cutting forces, chip morphology and temperature distribution, including the peak temperatures generated during the process. By optimizing the numerical and material parameters, we achieved a relative error on cutting forces below 11% across all cases when comparing our model predictions to the full set of experimental data from the literature presented here.

KEYWORDS

Fracture energy; machining; numerical model; temperature prediction; Ti6Al4V

Introduction

Ti6Al4V is a highly sought-after material in the automotive, aeronautical and medical industries due to its combination of excellent mechanical properties, biocompatibility, corrosion resistance and low thermal conductivity (Sun et al., 2009; Li et al., 2019). However, its low machinability makes machining Ti alloys a challenge, as it requires high cutting forces and results in severe tool wear (Yang et al., 2022).

Cutting tool wear is an important consideration in the machining of Ti6Al4V, as it can significantly affect the quality, efficiency and cost of the process. Wear is the gradual loss of material from the cutting tool's surface due to repeated contact with the workpiece. In machining, wear

CONTACT X. Soldani xsoldani@comillas.edu Department of Mechanical Engineering - ICAI, Universidad Pontificia Comillas, Madrid, Spain.

mechanisms are primarily caused by the combination of high temperatures and mechanical stresses generated at the cutting edge (Komanduri and von Turkovich, 1981; Ramírez et al., 2017).

To address these challenges, the optimization of cutting parameters and the selection of appropriate tool geometry and material are crucial elements in the machining process.

Over the past decades, a significant body of research has been conducted on machining Ti6Al4V, both through experimental and numerical works. These studies have contributed to a deeper understanding of the prediction of tool wear (Ramírez et al., 2017; Yang et al., 2022), the mechanisms of chip formation (Hoffmeister et al., 1999; Gente et al., 2001), the determination of cutting forces (Molinari et al., 2002; Li et al., 2019), the calculation of residual stresses in the workpiece (Niesłony et al., 2014; Shi et al., 2022), or the temperature distribution (Chen et al., 2011; Garcia-Gonzalez et al., 2016).

One of the earliest experimental tests on machining of Ti6Al4V was carried out by Komanduri and von Turkovich (1981) in 1981 at cutting speeds below 5 m/s to investigate the impact of cutting conditions on shear band formation. In 1999 and 2001, Hoffmeister et al. (1999) and Gente et al. (2001) investigated the chip formation in orthogonal cutting in a large range of cutting speeds (from 5 m/s to 100 m/s) and concluded that chip segmentation is not caused by catastrophic adiabatic shear but by crack propagation. In 2002, Molinari et al. (2002) presented experimental work on orthogonal cutting applied to titanium alloy, observing that cutting velocity strongly affects strain localization and the adiabatic shear banding may induce phase transformation. They also found that the frequency of segmentation and the width of the shear band are directly proportional to the cutting speed and feed rate. This finding was also supported by the image analysis of machining tests performed by Cotterell and Byrne (2008) in 2008, as well as the study conducted by Sun et al. (2009) in 2009, which concluded that the frequency of shear banding is directly proportional to the cutting speed and inversely proportional to the feed rate. In 2014, Ducobu et al. (2014) showed experimentally and numerically that the saw-toothed chip is due to the combination of adiabatic shear banding in the primary shear zone and the propagation of a crack into it. In 2019, Li et al. (2019) studied experimentally the effect of nanofluids as lubrication on the cutting forces and chip morphology; they showed how the percentage of nanofluids can reduce the energy necessary. In 2022, Yang et al. (2022) performed an orthogonal cutting experience with an LPEB-irradiated tool, analyzing tool flank wear through chip morphology, contact length measurement and output friction coefficient. In 2022, Outeiro et al. (2022) carried out experimental cutting tests using coated and uncoated WC tools to

measure cutting forces and study chip morphology; they coupled their experimental work with machine learning methods to predict the residual stresses for other cutting conditions.

Bäker (2005), Bäker et al. (2002) and Bäker et al. (2003) conducted numerical studies on orthogonal cutting and showed that the mechanical and thermal behavior of the material plays a significant role in the formation and propagation of shear bands. Specifically, numerical studies revealed that materials with higher hardening tend to undergo segmentation only at very high cutting speeds, whereas stronger thermal softening promotes the formation of shear bands at lower cutting velocities. Furthermore, the authors investigated the impact of thermal conductivity on the segmentation phenomenon and found that higher thermal conductivity is associated with lower segmentation intensity. Umbrello (2008) investigated the impact of rheological parameters on cutting forces and chip morphology. In 2008, Calamaz et al. (2008) developed and applied an original material constitutive law for Ti alloy within finite element software and looked at the effect of mechanical properties such as strain hardening, strain rate sensitivity and thermal softening on chip segmentation. In 2010, Karpat (2010) developed a modified material model for Ti-6Al-4V that accounts for the interactions between strain, strain rate and temperature. The model captures the material's flow softening behavior at high strains, and a parametric analysis is performed to evaluate the influence of model parameters on the finite element simulation result. In 2010, Sima and Özel (2010) showed that flow-softening increases the intensity of chip serration and segmentation. In 2011, through their numerical work, Chen et al. (2011) predicted the distribution of strain, stress and temperature in the chip during the machining of Ti6Al4V, revealing that thermal softening becomes the dominant factor in the presence of strain hardening along the shear band, while between two shear bands, strain hardening prevails over thermal softening. Miguélez et al. (2013) and Molinari et al. (2013) studied the initiation and propagation of shear bands in titanium machining. The authors focused on the effects of material parameters, friction coefficient and cutting conditions. In 2015, Jagadesh and Samuel (2015) proposed a finite element model, using various shear friction factors, that is developed and calibrated using experimental data to rigorously validate and support the interpretations derived from the mechanistic model. They showed that the strain rate increases with higher cutting speeds, while it decreases with increasing feed rate due to the wider spacing of adiabatic shear bands. The influence of both constitutive law and the separation criterion on cutting forces and chip morphology was also investigated by Ducobu et al. (2016) in 2016. The study showed that the cutting forces are mainly affected by the

constitutive law, while the chip morphology is primarily controlled by the chip separation criterion. In 2017, Soldani et al. (2017) studied the influence of fracture energy on numerical outputs in machining; they showed that fracture energy has a significant impact on predictions of cutting forces and chip morphology. In 2019, Soldani and López-Gálvez (2019) proposed an original model of orthogonal cutting using cohesive elements to separate the chip from the machined workpiece to avoid the use of a sacrificial layer. In 2022, Lois-Dorothy et al. (2022), the authors carried out numerical work in Abaqus to study the influence of fracture strain and inelastic heat friction on shear band initiation and propagation. In 2024, Zhang et al. (2024) employed a hybrid SPH-FEM model to investigate the role of friction, with particular emphasis on its effect at the tool-chip interface exit zone on chip formation. The work provides a detailed analysis of the evolution of key physical parameters, namely normal contact pressure, sliding velocity and temperature-dependent friction, based on friction models available in literature. In 2024, Mustafa et al. (2024) studied, through a numerical model developed with Abaqus/Explicit, the effects of preheating temperature on the cutting force, cutting zone temperatures and chip morphology. In 2025, Hu et al. (2025) investigated the machining-induced plastic strain on the workpiece surface using a combined experimental and numerical methodology. In their work, a complete simulation sequence—including cutting, unloading and cooling phases—was developed by coupling Abaqus Explicit and Implicit solvers, enabling a more accurate prediction of the residual plastic deformation generated by the machining process. In 2025, Sahu and Jha (2025) presented a finite element model based on a moving Gaussian heat source to simulate laser micromilling of Ti6Al4V, incorporating phase change phenomena and validated by experimental measurements of microgroove geometry.

The article is focused on the optimization of a numerical model of orthogonal cutting applied to Ti6Al4V. The novelty and main contributions of this study can be summarized as follows:

- A comprehensive determination and calibration of all key input parameters for high-speed orthogonal cutting of Ti6Al4V, including:
  - Numerical parameters: mesh size and mass scaling factor.
  - Tribological parameters: tool–chip friction coefficient.
  - Material parameters: fracture energy of Ti6Al4V over a wide range of cutting speeds.
- Development of a validated finite element model using Abaqus that accurately predicts cutting forces, chip morphology and temperature distribution in high-speed machining conditions.

- Achievement of a relative error below 11% when comparing numerical predictions to experimental data from the literature, demonstrating the robustness and reliability of the proposed modeling approach.
- Contribution to the reduction of expensive experimental trials by providing a numerically efficient and physically consistent framework for simulating titanium alloy machining.

Numerical model

The Lagrangian approach effectively captures various chip morphologies, including continuous, segmented and fragmented forms. The main drawback of the approach is due to the strong deformations that the elements of the model undergo. These high strain values generated in the chip can lead to some calculation errors and element distortions. To reproduce the material behavior as faithfully as possible and to minimize possible problems of distortions, a damage model was implemented in the orthogonal cutting simulation.

Geometry and boundary conditions

The model presented in this article is a two-dimensional simulation of orthogonal cutting under the plane strain assumption; it was developed with the finite element code ABAQUS/Explicit using a Lagrangian formulation. The elements used in the machined and tool parts are quadrilateral, 4-node, bilinear, plane strain and thermally coupled with a reduced integration (CPE4RT denomination). The geometry, dimensions and boundary conditions are summarized in Figure 1.

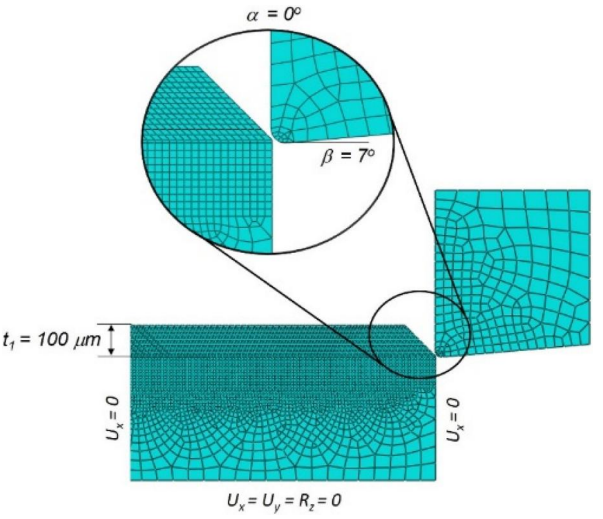

Figure 1. Geometry and boundary conditions of the orthogonal cutting model.

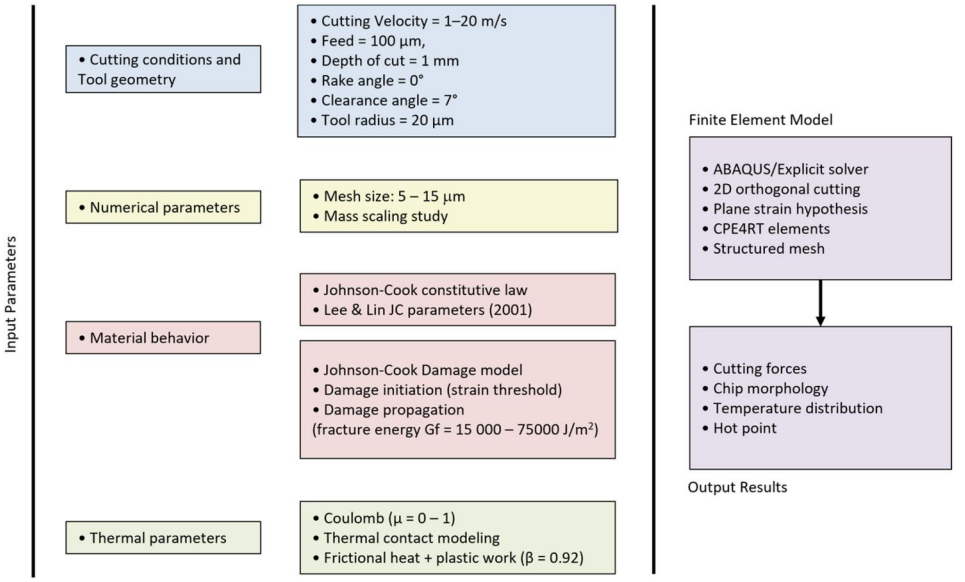

Figure 2. Diagram of parameters implemented in the study.

In the simulation, the cutting velocity is applied to the tool (V_c ranges from 1 to 20 m/s), and the workpiece displacements and rotation are constrained at its boundaries. All calculations were performed for constant values of feed ($t_1 = 100\,\mu$m), tool rake angle ($\alpha = 0^\circ$), clearance angle ($\beta = 7^\circ$) and cutting-edge radius ($r = 20\,\mu$m). As the numerical calculations are two-dimensional, the depth of cut p is assumed to be $p = 1$ mm.

To facilitate the understanding of the constants and variables analyzed in this study, the following diagram is proposed (Figure 2):

Mechanical properties

The tool is supposed to be totally rigid, and the machined material is assumed to be isotropic and elastoviscoplastic and follows the J_2 flow theory (von-Misès yield criterion). To characterize the material's behavior, the Johnson-Cook law, (1), was selected (Johnson and Cook, 1983).

$$\sigma = \left(A + B\varepsilon_p^n\right)\left(1 + Cln\frac{\dot{\varepsilon_p}}{\dot{\varepsilon}_0}\right)\left(1 - \left(\frac{\mathrm{T} - T_0}{T_m - T_0}\right)^m\right) \tag{1}$$

where σ, ε_p and $\dot{\varepsilon_p}$ are, respectively, the tensile flow stress, the plastic strain and the equivalent plastic strain rate. T defines the absolute temperature; T_0 and T_m represent, respectively, the reference and the melting temperature of the material ($T_m = 1673$ K). The constitutive law parameters were calibrated by Lee and Lin (Lee and Lin, 1998) for a referential strain rate

Table 1. Johnson-Cook parameters for Ti6Al4V (Lee and Lin n.d.).

Johnson-Cook parameters				
A (MPa)	*B* (Mpa)	*n*	*c*	*m*
782	498	0.28	0.028	1

Table 2. Mechanical properties for Ti6Al4V.

Mechanical properties	
Density ρ (kg/m^3)	4420
Poisson ratio ν	0.3
Modulos of Elasticity *E* (GPa)	114

$\dot{\varepsilon}_0 = 10^{-5}$ s^{-1}. Their values are summarized in Table 1. The other mechanical parameters for Ti6Al4V (Young's modulus E, density ρ and Poisson's coefficient ν) are shown in Table 2.

Thermal properties and tool/chip interface considerations

Friction at the tool/chip interface and plastic work are the two main contributions to heating in chip-removal processes. In the simulation, both contributions have been considered. The contact at the tool rake face is described by the Coulomb friction law. Zhang et al. (2024) implemented a high-resolution hybrid SPH–FEM solver to model Ti6Al4V orthogonal cutting and confirmed that using a constant Coulomb friction model yields strong agreement with experimental cutting forces and chip shapes, as long as the friction coefficient remains within the realistic interval of $0 \leq \mu \leq 1$. Palanisamy et al. (2022) conducted 2D finite element simulations of orthogonal cutting of Ti6Al4V using an ALE (Arbitrary Lagrangian–Eulerian) formulation and demonstrated that, even with its simplicity, a constant Coulomb friction law effectively captures the tool–chip interface behavior, provided the friction coefficient is chosen between 0 and 1. In this article, the effect of the friction coefficient μ on numerical results (cutting forces, chip morphology and contact length) is studied; values from 0 to 1 have been implemented in the numerical simulations.

The plastic work contribution is given by the local form of the heat equation, which can be written as (2).

$$\rho C_p \dot{T} - k\Delta T = \beta \overline{\sigma_y} \dot{\varepsilon}_p \tag{2}$$

where $\dot{T}$ and ΔT are, respectively, the heating rate and the Laplacian of temperature. ρ, Cp and k define the mass density, the specific heat and the thermal conductivity; their values are given in Tables 2 and 3. $\overline{\sigma_y}$ *and* $\dot{\varepsilon}_p$ define the equivalent yield stress and the plastic strain rate.

The Taylor-Quinney coefficient β is a dimensionless material parameter that represents the fraction of plastic work converted into heat during plastic

Table 3. Thermal properties for Ti6Al4V (Mason et al. 1994).

Thermal properties	
Thermal conductivity k (W/m/K)	7.2
Specific heat capacity C_p (J/Kg/K)	560
Thermal expansion (/K)	$9.2e^{-6}$

deformation. Although it has been shown that the Taylor-Quinney coefficient is strain and strain rate dependent (Mason et al., 1994; Longère and Dragon, 2008, 2009), we assumed a constant value for β in this work. Experimental investigations by Rittel et al. (2017), which employed dynamic tension, compression and shear loading on commercially pure titanium (strain rates up to 10^3 s^{-1}), along with Smith et al. (2019), who performed high-speed tensile tests (up to 7000s^{-1}) on Ti-6Al-4V using digital image correlation and infrared thermography, have demonstrated that the Taylor–Quinney coefficient for titanium alloys typically lies between 0.9 and 0.95. Based on these considerations, a β value of 0.92 was used in our simulations.

Damage model

In machining simulations, various damage models can be used to define the type of damage in the material. The most common damage models implemented in chip removal calculations are: 1/Johnson-Cook damage model; this model is widely used to predict the damage caused by material deformation and fracture due to high strain rates and high temperatures. It considers material properties, such as strain rate sensitivity, strain hardening, thermal softening and thermal expansion (Calamaz et al., 2008; Soldani et al., 2017). 2/Damage accumulation model; it tracks the amount of damage that accumulates in the material due to various mechanisms such as plastic deformation, fatigue and fracture. The damage accumulation can be quantified using different parameters such as the accumulated plastic strain, accumulated fatigue cycles and accumulated crack length. 3/Cohesive zone model; it is used to simulate fracture in the material. It considers the separation and sliding of material along the crack surfaces and the associated energy dissipation (Soldani and López-Gálvez, 2019). The cohesive zone model is particularly useful for simulating crack propagation in brittle materials.

In this article, the Johnson-Cook damage model has been implemented in the simulation. In the formulation, the damage process can be divided into two steps: damage initiation and propagation (Figure 3) (Mason et al., 1994).

Damage initiation

The initiation of damage begins when the equivalent plastic stress reaches $\sigma = \sigma_{yo}$. Indeed, from this threshold value, the damage W is then calculated

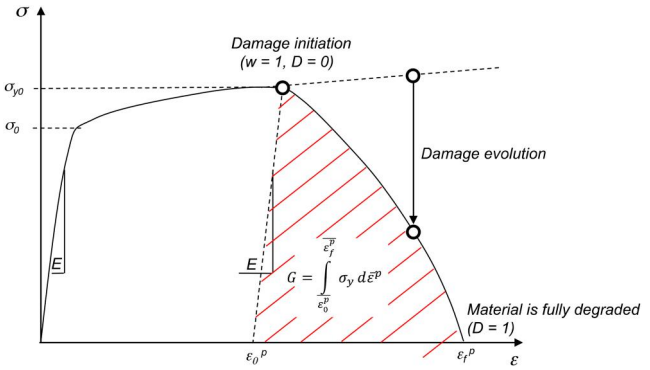

Figure 3. Effects of damage on flow stress and definition of the fracture energy G.

Table 4. Johnson-Cook damage parameters for Ti6Al4V (Johnson et al. 1989).

Johnson-Cook damage parameters				
D1	*D2*	*D3*	*D4*	*D5*
−0.09	0.25	−0.5	0.014	3.87

for each element of the workpiece through Equation (3):

$$W = \sum \frac{\Delta \bar{\varepsilon}^p}{\bar{\varepsilon}_0^p} \tag{3}$$

where $\Delta \bar{\varepsilon}^p$ and $\bar{\varepsilon}_0^p$ are, respectively, the increment of equivalent plastic strain and the threshold equivalent plastic strain.

The threshold equivalent plastic strain is thus calculated by Equation (4):

$$\bar{\varepsilon}_0^p = \left[D_1 + D_2 \exp(D_3 \sigma^*)\right] \left[1 + D_4 ln \frac{\dot{\varepsilon}}{\dot{\varepsilon}_0}\right] \left[1 - D_5 \left(\frac{T - T_0}{T_f - T_0}\right)\right] \tag{4}$$

where $\bar{\varepsilon}_0^p$ is calculated from the parameters D_i ($i = 1$ – 5), calibrated from experimental observations, and based on the determination of the triaxiality ratio σ^* (first term of the equation); their values are summarized in Table 4 (Johnson and Cook, 1985). The second and the third terms of the equation define the strain rate and temperature sensitivity. The rate of triaxiality is given by relation (5):

$$\sigma^* = \frac{\sigma_m}{\bar{\sigma}} \tag{5}$$

with σ_m, the average normal stresses and $\bar{\sigma}$ the von Mises equivalent plastic stress.

Damage propagation

The Johnson-Cook damage propagation is governed by an energetic criterion using the element fracture energy G_f of the material, described by Equation (6):

$$G_f = L_e \times G = L_e \int_{\overline{\varepsilon}_0^p}^{\overline{\varepsilon}_f^p} \sigma_y d\overline{\varepsilon}^p \tag{6}$$

where L_e defines the characteristic length of the element.

To correctly use this type of formulation, it is therefore essential to have a constant mesh size throughout the part undergoing damage. In our calculations, we used a structured mesh in the workpiece part, giving a constant element characteristic length for each simulation. In addition, the calibration of the fracture energy is a key point of the model presented in this article. In the paragraph on Fracture energy analysis, the calibration and experimental validation of the element fracture energy G_f are presented.

Numerical results and validation

In this section, a systematic study of the key parameters influencing the numerical model of orthogonal cutting applied to Ti6Al4V is presented. Each parameter—mesh size (Mesh size analysis), mass scaling factor (Mass scaling analysis), friction coefficient at the tool/chip interface (Friction coefficient analysis) and fracture energy of the material (Fracture energy analysis)—will be carefully analyzed to determine its optimal value. The objective is to calibrate these parameters to improve the accuracy and robustness of the numerical simulations. This thorough investigation enables us to validate the model against experimental data and ensure its predictive reliability across a wide range of cutting conditions.

Mesh size analysis

Mesh size optimization is a critical balance between achieving numerical accuracy and controlling computational cost. It requires precise calibration to ensure the fidelity of simulation results while optimizing simulation efficiency. Convergence criteria are used to determine when the simulation has reached a solution that is acceptable in terms of accuracy and stability.

In this part, calculations with a mesh size of 5, 8, 10 and 15 μm have been performed; a comparison in terms of specific cutting and thrust forces ($\frac{F_c}{t_1.p}$ and $\frac{F_t}{t_1.p}$) is presented in Figure 4.

First, it can be easily observed that between the coarsest mesh 15 μm (computational time $C_t = 29$ min) and the 10 μm mesh size ($C_t = 69$ min), the specific cutting forces do not converge. From 10 μm mesh calculations, the specific cutting force appears to stabilize around 2552 N/mm^2. However, the specific thrust force still decreases; indeed, for the calculations carried out at 10 and 8 μm ($C_t = 151$ min), $\frac{F_t}{t_1.p}$ reduces from 2009 to

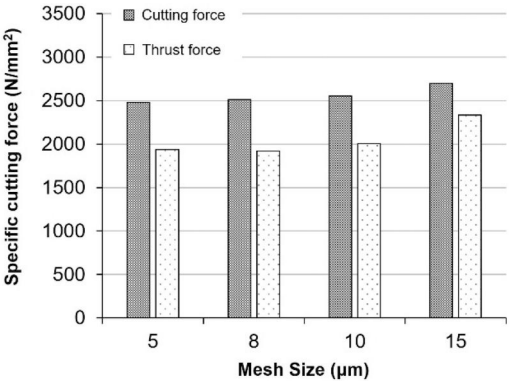

Figure 4. Effect of mesh size on numerical cutting and thrust forces. ($V_C = 3$ m/s – $G_f = 45\,000$ J/m^2).

1919 N/mm^2. Numerical simulations performed with the finest mesh size 5 μm ($C_t = 301$ min) show that the specific cutting and feed forces both stabilize.

Therefore, from these considerations, all numerical calculations in this article were carried out for the 8 μm mesh size.

Mass scaling analysis

In Explicit numerical simulations, the computational time C_t is determined by the step time δ_t, indexed on the elastic wave speed in the material; the Courant-Friedrichs-Lewy condition is presented in relation (7):

$$\delta_t \leq f.L_e\sqrt{\frac{\rho}{E}} \tag{7}$$

where f defines the factor scale (0.9), L_e the characteristic length of the element, E the Young's modulus and ρ the material density.

As shown in Equation (7), increasing the density ρ, the time step is reduced; the concept of the mass scaling factor is based on this numerical consideration. In Abaqus it is possible to artificially modify the mass of the material for the smallest elements to reduce the overall calculation time of the simulation; in thermodynamic calculations, such as machining processes, the method can become extremely useful. However, altering the time step must be done carefully in order not to distort the numerical results.

Figure 5 presents the effects of mass scaling on numerical predictions of specific cutting forces and morphology for a tool cutting velocity $V_C = 3$ m/s. An excessive increase in the step time (from $\delta_t = 1e^{-11}$ s to $\delta_t = 1e^{-9}$ s) significantly affects the cutting forces as well as the geometry of the chip; indeed, for this larger step time ($\delta_t = 1e^{-9}$ s), a reduction in cutting forces of around 15% is observed, together with a much more pronounced

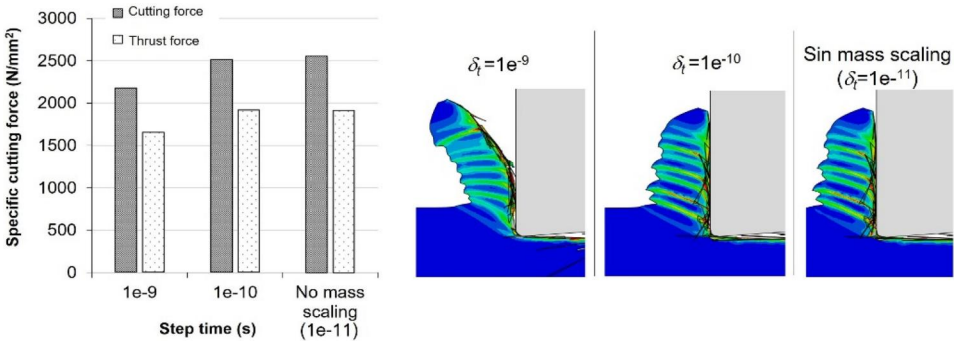

Figure 5. Effect of mass scaling on specific cutting forces and chip morphology. (V_C = 3 m/s – G_f = 45 000 J/m^2).

chip curvature. When using a step time $\delta_t = 1e^{-10}$ s the numerical outputs are not modified; the computational time C_t is then reduced by approximately 10%. Therefore, all calculations were carried out for a step time $\delta_t = 1e^{-10}$.

Friction coefficient analysis

The contact at the tool/chip interface was modeled using the Coulomb friction law. The Coulomb law can reproduce complex contact phenomena at the tool-chip interface, including sticking near the tool tip due to thermal softening and sliding friction along the rest of the tool-chip interface. In machining of Ti6Al4V, the average friction coefficient μ at the tool chip interface ranges from 0.3 to 0.8, depending on the cutting conditions (Johnson and Holmquist, 1989; Romero, 2016; Afrasiabi et al., 2021).

In this part, a parametric study on friction coefficient μ is presented; we carried out simulations at different cutting velocities (from 1 to 20 m/s) for a large range of values of μ = 0, 0.25, 0.5, 0.8 and 1. The specific cutting forces and chip morphologies obtained are shown, respectively, in Figures 6 and 7.

For the entire range of cutting velocities, friction has a significant effect on the numerical specific forces shown in Figure 6. This effect is especially pronounced at lower cutting speeds. For instance, at V_C = 1 m/s, the specific cutting force goes from 1900 N/mm^2 to 2800 N/mm^2 by changing μ from 0 to 1. At low cutting speed ($V_C \leq$ 5 m/s), the temperature at the tool/chip interface is inferior, and the effect of the friction coefficient is, in proportion, more significant. In this case ($1 \leq V_C \leq$ 5 m/s), a small variation of the friction coefficient value induces a large deviation of cutting forces; the different slopes of specific cutting forces, for each friction coefficient, clearly show its effect. Conversely, for higher cutting speeds ($V_C \geq$ 5 m/s), the effect of friction is lower: for V_C = 20 m/s), the specific cutting force

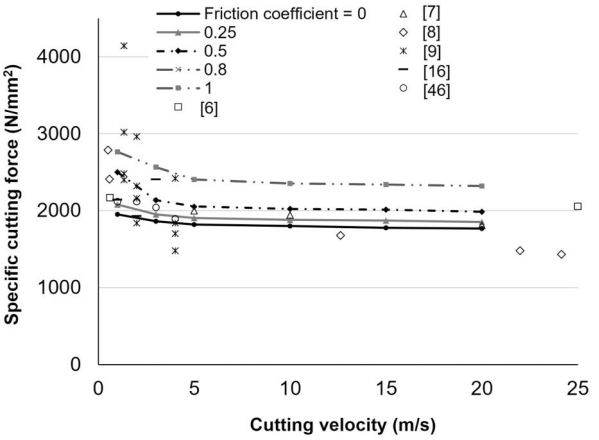

Figure 6. Effect of friction coefficient on specific cutting forces for different cutting velocities and experimental comparison.
($G_f = 45\ 000$ J/m^2).

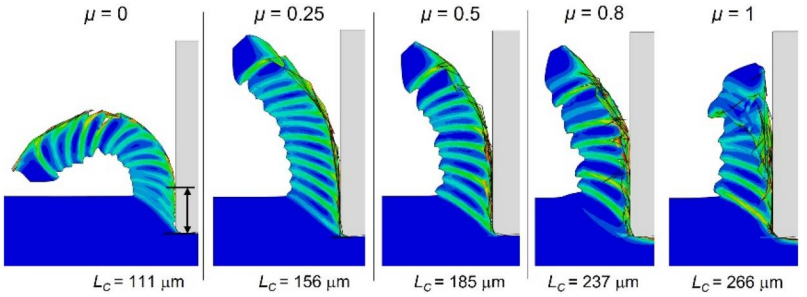

Figure 7. Effect of friction coefficient on chip morphology and contact length.
($V_C = 3$ m/s – $G_f = 45\ 000$ J/m^2).

goes from 1820 N/mm^2 to 2340 N/mm^2 by changing μ from 0 to 1. This observation can be explained by the high temperatures generated at the interface (for these velocities), inducing a saturation of the thermal softening, which tends to reduce slightly the importance of the friction coefficient.

A comparison with experimental measurements of the specific forces obtained in the orthogonal cutting process by Johnson and Holmquist (1989); Hoffmeister et al. (1999); Gente et al. (2001); Molinari et al. (2002); Li et al. (2019); Outeiro et al. (2022) is made in Figure 5. Hoffmeister et al. (1999), Gente et al. (2001), Molinari et al. (2002) and Romero (Outeiro et al., 2022) carried out experimental investigations considering a tool rake angle $\alpha = 0°$; it can be noticed that in Hoffmeister et al. (1999); Gente et al. (2001); Molinari et al. (2002), the authors performed experimental cutting for a very large range of velocities. Li et al. (2019) studied the effect of lubrication by nanofluids on cutting forces for $\alpha = 6°$ and velocities ranging

from 1.3 to 4 m/s. Outeiro et al. (2022) investigated the effect of rake face value ($\alpha = -6°$ and 5°) on forces.

As numerical calculations, experimental measurements present two main trends: a first large decrease at low cutting speed and a slighter one for large velocities. It can be observed, in terms of absolute values, that numerical calculations performed with $\mu = 0.8$ show an excellent agreement with experimental measurement of specific cutting forces.

Chip morphologies obtained for different values of friction coefficient are presented in Figure 7. As expected, a higher value of μ induces a straighter chip morphology. Since the normal force to the rake face is higher, the curvature of the chip is reduced; this variation of the normal force also affects the tool/chip contact length L_C. Indeed, from the numerical simulations performed for the given cutting velocity $V_C = 3$ m/s, we measured L_C for the different configurations of friction coefficient. As observed, the contact length increases strongly and almost linearly with μ. The L_C value goes from 111 μm to 266 μm when the friction coefficient increases from 0 to 1.

Fracture energy analysis

The formation of the chip results from an intense shearing within a thin zone called the primary shear zone (PSZ). In the PSZ, the strain, strain rate and temperature can reach very high values. For usual typical machining cutting conditions, we can observe strain ranging between 3 and 6, strain rate between 10^3 and 10^5 s^{-1}, and temperature between 600 and 800 K in the primary shear zone. Under such extreme conditions, the fracture energy of the material can be estimated by evaluating the area under the true stress–strain curve, which corresponds to the energy absorbed by the material up to failure. Based on these conditions, it is possible to estimate the fracture energy in the chip during machining. Indeed, G can be calculated from the flow behavior of the material under conditions of strain, strain rate and temperature through the Johnson-Cook phenomenological law (Equation (1)); for these conditions, the fracture energy G ranges from 3000 MPa to 8500 MPa. Then, using Equation (6) and considering a characteristic length of 8 μm, the element fracture energy Gf goes from 24 000 J/m^2 to 69 000 J/m^2.

In this article, we performed numerical calculations for values of element fracture energy Gf = 15,000, 30,000, 45,000, 60,000 and 75,000 J/m^2. Figures 7 and 8 show the effect of the implemented energy Gf on cutting forces and chip morphology, respectively.

To correctly calibrate the Gf value, a comparison with experimental works of Johnson and Holmquist (1989); Hoffmeister et al. (1999); Gente et al. (2001); Molinari et al. (2002); Li et al. (2019); Outeiro et al. (2022) is

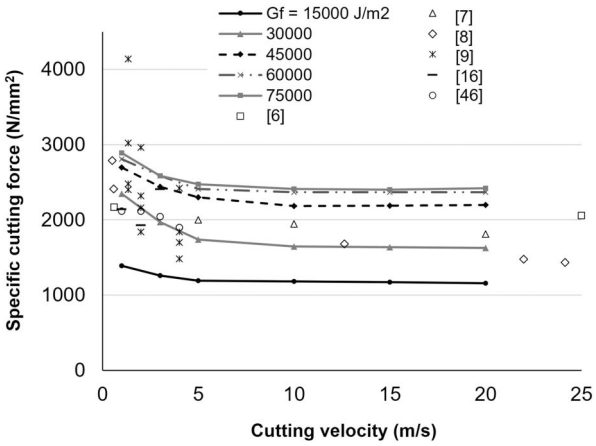

Figure 8. Effect of element fracture energy G_f on cutting forces and experimental comparison. ($V_C = 3$ m/s – $\mu = 0.8$).

presented. Note that all the experimental data summarized here were obtained in pure orthogonal cutting processes applied to Ti6Al4V. However, experimental forces presented in Figure 8 show differences in terms of absolute value; these variations are likely due to several hypotheses: the grade of the titanium alloy may be different; the rake angle is non-zero for Li et al. (2019) and Outeiro et al. (2022); the lubrication (using various percentages of nanofluids) differs. Nevertheless, as observed here and previously commented on the section "Friction coefficient analysis", the experimental measurements and numerical calculations show the same trend: a large decrease of the specific force for $V_C \leq 5$ m/s and an almost constant variation when $V_C \geq 5$ m/s.

By analyzing the specific cutting forces, it can be easily seen that the numerical simulations carried out for $Gf = 30\,000$ and $45\,000$ J/m^2 fit much better than for the other values of fracture energy. Indeed, the absolute values predicted by the numerical model as the curve trend are accurately reproduced here; the average difference between experimental values and numerical predictions is less than 11% for a fracture energy value of 30,000 and less than 14% when considering a fracture energy of $45\,000$ J/m^2.

Figure 9 presents the effects of fracture energy values on chip morphology considering a cutting velocity $V_C = 3$ m/s and a friction coefficient $\mu = 0.8$; the chip serration and chip curvature are analyzed here. It can be observed that at the lowest element fracture energy value, $G_f = 15{,}000$ J/m^2, the total segmentation of the chip. Each shear band leads to a complete fracture of the chip. For implemented element fracture energies of $G_f = 30{,}000$ and $45{,}000$ J/m^2 the chip flow behavior becomes more stable: indeed, the chip does not show complete segmentation but clearly presents some intense shear bands. For the highest values of the element fracture

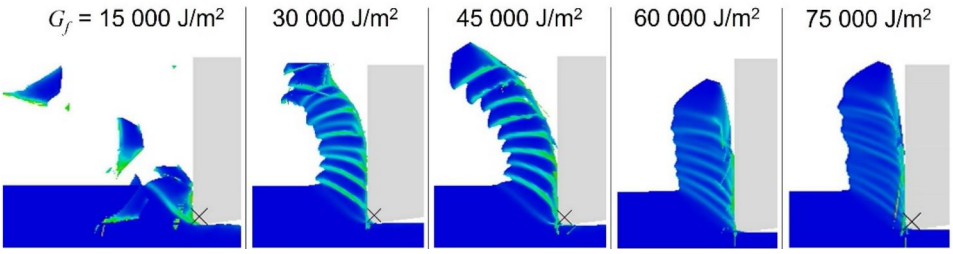

Figure 9. Variation of chip segmentation and curvature with element fracture energy G_f. (V_C = 3 m/s – μ = 0.8).

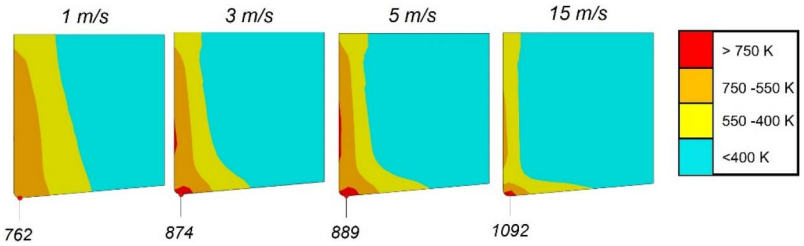

Figure 10. Temperature distribution at the tool rake face at 1.8 mm of machining length. (μ = 0.8 – G_f = 45 000 J/m²).

energy, G_f =60,000 and 75,000 J/m^2, the shearing is less severe and no complete propagation of the band is observed. Moreover, in these cases, the chip curvature radius is clearly lower.

Temperature analysis

It is well known that tool wear is drastically affected by a combined effect of temperature, pressure, abrasive particles and mechanical and thermal cracks or chip hammering (Hoffmeister et al., 1999; Ramírez et al., 2017). In materials such as Ti6Al4V, where the thermal conductivity is very low, the generated temperature has a strong effect on tool wear. Numerical calculations allow access to local data difficult to measure, such as temperature gradient during the cutting process.

In this section is presented the numerical results of temperature distribution and its maximum value T_{max} for various cutting velocities (considering a constant machined length).

Looking at the temperature distribution in Figure 10, it can be observed that a lower velocity shows a larger propagation of temperature on the tool rake face for the same cutting length. Indeed, the heat generated by friction has more time to deeply propagate into the tool. For V_C = 1 m/s, the average temperature on the tool rake face is around 650 K. For V_C = 3 and 5 m/s, the average temperature increases to 700 K and 730 K, respectively. Considering the highest cutting velocity V_C = 15 m/s, the value goes to

850 K; however, it is important to notice in this case that the temperature is almost entirely superficial.

When focusing on the maximum temperature, we can observe that the position of the hot spot is situated on the tool flank. As previously, a higher value of cutting velocity induces a much more elevated value of T_{max}. Indeed, from $V_C = 1$ m/s to 15 m/s, the maximum temperature T_{max} increases from 762 K to 1092 K; this last corresponds to 65% of the melting temperature T_m of the material, even well higher than the temperature of recrystallization of the Ti6Al4V material.

Conclusions

In this article is presented a new finite element model of orthogonal cutting applied to the Ti6Al4V alloy, with a particular focus on the systematic determination of all key model parameters. This includes the calibration of numerical parameters (mesh size and mass scaling factor), tribological parameters (friction coefficient at the tool/chip interface) and material parameters (fracture energy of Ti6Al4V), across a wide range of cutting speeds. This comprehensive approach aims to enhance the reliability and predictive accuracy of the model for high-speed machining simulations.

- Numerical parameters: mesh size and mass scaling factor.
- Tribological parameters: friction coefficient at the tool/chip interface.
- Material parameters: element fracture energy of Ti6Al4V.
- All these were evaluated across a wide range of cutting speeds, with the goal of improving the model's reliability and predictive capabilities for high-speed machining simulations.

1/Mesh size is a critical parameter in numerical simulations:

- For the considered geometry (feed rate $t_1 = 100$ µm), a mesh size of 8 µm showed good convergence of cutting force predictions.
- This setup also demonstrated the model's ability to accurately reproduce shear band localization and chip segmentation, which are key features in Ti6Al4V machining.

2/Machining is a highly dynamic and thermally coupled process, often resulting in very long computation times:

- To reduce these times, we conducted a study on the effect of the mass scaling factor.

- It was shown that increasing the time step (via controlled mass scaling) can significantly reduce computational time without affecting the quality of the numerical results.

3/The friction coefficient at the tool/chip interface is a major input affecting simulation accuracy:

- It strongly influences cutting forces, contact length, and chip shape.
- Through extensive comparison with experimental data from the literature, a value of $\mu = 0.8$ provided very good agreement in terms of specific cutting forces.

4/The element fracture energy of the material is essential for simulating material failure in the cutting zone:

- A parametric study allowed us to estimate the fracture energy of Ti6Al4V under orthogonal cutting conditions.
- For the mesh size and cutting speed range used, values were found to range between 30,000 and 45,000 J/m^2, consistent with experimental observations.

5/The temperature at the tool/chip interface is a key factor in wear prediction:

- The model enabled us to analyze the influence of cutting speed on temperature distribution, maximum temperature and hot spot location.
- The average temperature at the interface ranged from 650 K to 850 K, and interestingly, the hot spot was not located on the rake face but rather on the flank face, which has implications for tool wear mechanisms and tool design.

Disclosure statement

No potential conflict of interest was reported by the author(s).

References

Afrasiabi, M.; Berger, S.; Iovkov, I.; Klippel, H.; Röthlin, M.; Zabel, A.; Biermann, D.; Wegener, K. (2021) A numerical-experimental study on orthogonal cutting of AISI 1045 steel and Ti6Al4V alloy: SPH and FEM modeling with newly identified. Friction coefficients. *Metals* 11-11: 1683.

Bäker, M. (2005) Finite element investigation of the flow stress dependence of chip formation. *Journal of Materials Processing Technology*. 167(1): 1–13. doi:10.1016/j.jmatprotec.2004.09.076

Bäker, M.; Rösler, J.; Siemers, C. (2002) Finite element model of high speed metal cutting with adiabatic shearing. *Computers and Structures*. 80(5-6): 495–513. doi:10.1016/S0045-7949(02)00023-8

Bäker, M.; Rösler, J.; Siemers, C. (2003) The influence of thermal conductivity on segmented chip formation. *Computational Materials Science*. 26: 175–182. doi:10.1016/S0927-0256(02)00396-8

Calamaz, M.; Coupard, D.; Girot, F. (2008) A new material model for 2D numerical simulation of serrated chip formation when machining titanium alloy Ti–6Al–4V. *International Journal of Machine Tools and Manufacture* 48(3-4): 275–288. doi:10.1016/j.ijmachtools.2007.10.014

Chen, G.; Ren, C.; Yang, X.; Jin, X.; Guo, T. (2011) Finite element simulation of high-speed machining of titanium alloy (Ti–6Al–4V) based on ductile failure model. *The International Journal of Advanced Manufacturing Technology* 56(9–12): 1027–1038. doi:10.1007/s00170-011-3233-6

Cotterell, M.; Byrne, G. (2008) Dynamics of chip formation during orthogonal cutting of titanium alloy Ti–6Al–4V. *CIRP Annals* 57(1): 93–96. doi:10.1016/j.cirp.2008.03.007

Ducobu, F.; Rivière-Lorphèvre, E.; Filippi, E. (2014) Numerical contribution to the comprehension of saw-toothed Ti6Al4V chip formation in orthogonal cutting. *International Journal of Mechanical Sciences* 81: 77–87. doi:10.1016/j.ijmecsci.2014.02.017

Ducobu, F.; Rivière-Lorphèvre, E.; Filippi, E. (2016) Material constitutive model and chip separation criterion influence on the modeling of Ti6Al4V machining with experimental validation in strictly orthogonal cutting condition. *International Journal of Mechanical Sciences* 107: 136–149. doi:10.1016/j.ijmecsci.2016.01.008

Garcia-Gonzalez, J.C.; Moscoso-Kingsley, W.; Madhavan, V. (2016) Tool rake face temperature distribution when machining Ti6Al4V and Inconel 718. *Procedia Manufacturing* 5: 1369–1381. doi:10.1016/j.promfg.2016.08.107

Gente, A.; Hoffmeister, H.-W.; Evans, C.J. (2001) Chip formation in machining Ti6Al4V at extremely high cutting speeds. *CIRP Annals* 50(1): 49–52. doi:10.1016/S0007-8506(07)62068-X

Hoffmeister, H.W.; Gente, A.; Weber, T. (1999) "Chip formation of titanium alloys", *Proceeding of 2nd International Conference on High Speed Machining, Darmstadt: Germany*, p. 21–8,

Hu, C.; Zhuang, K.; Elias-Birembaux, H.; Outeiro, J. (2025) An improved numerical model for prediction of residual plastic strain in machining of Ti6Al4V titanium alloy concerning cutting edge microgeometries. *Procedia CIRP* 133: 722–727. doi:10.1016/j.procir.2025.02.123

Jagadesh, T.; Samuel, G.L. (2015) Mechanistic and finite element model for prediction of cutting forces during micro-turning of titanium alloy. *Machining Science and Technology* 19(4): 593–629. doi:10.1080/10910344.2015.1085318

Johnson, G.; Holmquist, T. (1989) *Test data and computational strength and fracture model constants for 23 materials subjected to large strains, high strain rates, and high temperatures*. Los Alamos National Laboratory, Los Alamos.

Johnson, G.R.; Cook, W.H. (1983) "A constitutive model and data for metals subjected to large strains, high strain rates and high temperatures", *Proc. 7th Int. Symp. on Ballistics*, Netherlands, p. 541–547.

Johnson, G.R.; Cook, W.H. (1985) Fracture characteristics of three metals subjected to various strains, strain rates, temperatures and pressures. *Engineering Fracture Mechanics*. 21(1): 31–48. doi:10.1016/0013-7944(85)90052-9

Karpat, Y. (2010) A modified material model for the finite element simulation of machining titanium alloy Ti-6Al-4V. *Machining Science and Technology* 14(3): 390–410. doi:10.1080/10910344.2010.512499

Komanduri, R.; von Turkovich, B.F. (1981) New observations on the mechanism of chip formation when machining titanium alloys. *Wear* 69(2): 179–188. doi:10.1016/0043-1648(81)90242-8

Lee, W.S.; Lin, C.F. (1998) High-temperature deformation behaviour of Ti6Al4V alloy evaluated by high strain-rate compression tests. *Journal of Materials Processing Technology*. 75(1-3): 127–136. doi:10.1016/S0924-0136(97)00302-6

Li, G.; Yi, S.; Li, N.; Pan, W.; Wen, C.; Ding, S. (2019) Quantitative analysis of cooling and lubricating effects of graphene oxide nanofluids in machining titanium alloy Ti6Al4V. *Journal of Materials Processing Technology* 271: 584–598. doi:10.1016/j.jmatprotec.2019.04.035

Lois-Dorothy, H.; Soldani, X.; Longère, P. (2022) A parametric numerical study of ASB-assisted chip formation in high-speed machining of Ti-6Al-4V. *Advances in Materials and Processing Technologies* 8(4): 4452–4470. doi:10.1080/2374068X.2022.2077524

Longère, P.; Dragon, A. (2008) Evaluation of the inelastic heat fraction in the context of microstructure-supported dynamic plasticity modelling. *International Journal of Impact Engineering*. 35(9): 992–999. doi:10.1016/j.ijimpeng.2007.06.006

Longère, P.; Dragon, A. (2009) Inelastic heat fraction evaluation for engineering problems involving dynamic plastic localization phenomena. *Journal of Mechanics of Materials and Structures* 4(2): 319–349. doi:10.2140/jomms.2009.4.319

Mason, J.J.; Rosakis, A.J.; Ravichandran, G. (1994) On the strain and strain rate dependence of the fraction of plastic work converted to heat: an experimental study using high speed infrared detectors and the Kolsky bar. *Mechanics of Materials* 17(2-3): 135–145. doi:10.1016/0167-6636(94)90054-X

MatWeb LLC. (s.d.). Titanium Alloy Ti-6Al-4V, annealed: Mechanical properties. MatWeb. https://www.matweb.com

Miguélez, M.H.; Soldani, X.; Molinari, A. (2013) Analysis of adiabatic shear banding in orthogonal cutting of Ti alloy. *International Journal of Mechanical Sciences* 75: 212–222. doi:10.1016/j.ijmecsci.2013.06.011

Molinari, A.; Musquar, C.; Sutter, G. (2002) Adiabatic shear banding in high speed machining of Ti–6Al–4V: experiments and modeling. *International Journal of Plasticity* 18(4): 443–459. doi:10.1016/S0749-6419(01)00003-1

Molinari, A.; Soldani, X.; Miguélez, M.H. (2013) Adiabatic shear banding and scalling laws in chip formation with application to cutting of Ti-6Al-4V. *Journal of the Mechanics and Physics of Solids* 61(11): 2331–2359. doi:10.1016/j.jmps.2013.05.006

Mustafa, M.; Pervaiz, S.; Deiab, I. (2024) A novel finite element model for thermally induced machining of Ti6Al4V. *Simulation Modelling Practice and Theory* 134: 102928. doi:10.1016/j.simpat.2024.102928

Niesłony, P.; Grzesik, W.; Laskowski, P.; Sienawski, J. (2014) Numerical and experimental analysis of residual stresses generated in the machining of Ti6Al4V titanium alloy. *Procedia CIRP* 13: 78–83. doi:10.1016/j.procir.2014.04.014

Outeiro, J.; Cheng, W.; Chinesta, F.; Ammar, A. (2022) Modelling and optimization of machining of Ti-6Al-4V titanium alloy using machine learning and design of experiments methods. *Journal of Manufacturing and Materials Processing* 6(3): 58. doi:10.3390/jmmp6030058

Palanisamy, N.; Rivière-Lorphèvre, E.; Arrazola, P.-J.; Ducobu, F. (2022) Influence of Coulomb's friction coefficient in finite element modeling of orthogonal cutting of Ti6Al4V. *Key Engineering Materials* 926: 1619–1628. doi:10.4028/p-be47dp

Ramírez, P. F.; Soldani, X.; Loya, J.; Miguélez, H. (2017) A new approach for time-space wear modeling applied to machining tool wear. *Wear* 390-391: 125–134. doi:10.1016/j.wear.2017.07.015

Rittel, D.; Zhang, L.H.; Osovski, S. (2017) The dependence of the Taylor–Quinney coefficient on the dynamic loading mode. *Journal of the Mechanics and Physics of Solids* 107: 96–114. doi:10.1016/j.jmps.2017.06.016

Romero, J. M. (2016) Formulación de un algoritmo eficiente de integración de un modelo de daño isótropo y validación en condiciones dinámicas. PhD thesis.

Sahu, A.K.; Jha, S. (2025) Modeling and simulation of ablated profile in laser micro-milling process of Ti6Al4V. *Machining Science and Technology* 29(4): 465–487. doi:10.1080/10910344.2025.2480779

Shi, B.; Abboud, E.; Attia, M.H.; Thomson, V. (2022) Effect of chip segmentation on machining-induced residual stresses during turning of Ti6Al4V. *Procedia CIRP* 108: 424–429. doi:10.1016/j.procir.2022.03.066

Sima, M.; Özel, T. (2010) Modified material constitutive models for serrated chip formation simulations and experimental validation in machining of titanium alloy Ti–6Al–4V. *International Journal of Machine Tools and Manufacture* 50(11): 943–960. doi:10.1016/j.ijmachtools.2010.08.004

Smith, J.; D.; Seidt.; A.; Gilat. (2019) Full field determination of the Taylor Quinney coefficient in tension tests of Ti 6Al 4V at strain rates up to 7000 s^{-1}. *Advancement of Optical Methods & Digital Image Correlation in Experimental Mechanics* 3: 133–139.

Soldani, X.; López-Gálvez, H. (2019) Chip formation modeling using traction-separation cohesive model. *The International Journal of Advanced Manufacturing Technology* 101(1–4): 171–179. doi:10.1007/s00170-018-2940-7

Soldani, X.; López-Gálvez, H.; Díaz-Álvarez, J. (2017) Numerical modeling of instabilities during machining of aeronautical alloy. *Procedia Manufacturing* 13: 36–42. doi:10.1016/j.promfg.2017.09.006

Sun, S.; Brandt, M.; Dargusch, M.S. (2009) Characteristics of cutting forces and chip formation in machining of titanium alloys. *International Journal of Machine Tools and Manufacture* 49(7-8): 561–568. doi:10.1016/j.ijmachtools.2009.02.008

Umbrello, D. (2008) Finite element simulation of conventional and high speed machining of Ti6Al4V alloy. *Journal of Materials Processing Technology* 196(1–3): 79–87. doi:10.1016/j.jmatprotec.2007.05.007

Yang, S.M.; Choe, J.-H.; Kim, J.; Park, H.W.; Kim, D.Y. (2022) Improvement of tool life via unique surface modification of a tungsten carbide tool using a large pulsed electron beam in Ti-6Al-4V machining. *Journal of Manufacturing Processes* 83: 223–234. doi:10.1016/j.jmapro.2022.09.001

Zhang, N.; Klippel, H.; Kneubühler, F.; Afrasiabi, M.; Kuffa, M.; Wegener, K. (2024) Investigation of friction modeling on numerical Ti6Al4V cutting simulations. *International Journal of Mechanical Sciences* 274(15): 109231. doi:10.1016/j.ijmecsci.2024.109231